New Journal of Physics
The open access journal at the forefront of physics

Deutsche Physikalische Gesellschaft DPG IOP Institute of Physics

Multiple quantum oscillation frequencies in $YBa_2Cu_3O_{6+\delta}$ and bilayer splitting

New Journal of Physics
The open-access journal for physics

Multiple quantum oscillation frequencies in $YBa_2Cu_3O_{6+\delta}$ and bilayer splitting

David Garcia-Aldea and Sudip Chakravarty[1]
Department of Physics and Astronomy, University of California Los Angeles, Los Angeles, CA 90095-1547, USA
E-mail: sudip@physics.ucla.edu

New Journal of Physics **12** (2010) 105005 (24pp)
Received 27 April 2010
Published 29 October 2010
Online at http://www.njp.org/
doi:10.1088/1367-2630/12/10/105005

Abstract. Experiments have revealed multiple quantum oscillation frequencies in underdoped high-temperature superconductor $YBa_2Cu_3O_{6+\delta}$, corresponding to approximately 10% doping, which contains CuO bilayers in the unit cell. These unit cells are further coupled along the c-axis by a tunneling matrix element. A model of the energy dispersion that has its roots in the previously determined electronic structure, combined with twofold commensurate density waves, reveals multiple electron and hole pockets. To the extent that quasiparticles of the reconstructed Fermi surface have finite residues, however small, the formation of Landau levels is the cause of these oscillations, and the bilayer splitting and warping of the electronic dispersion along the direction perpendicular to the CuO-planes are firm consequences. The goal here is to explore this possibility from various directions and provide a better understanding of the rapidly developing experimental situation involving multiple frequencies. An important conclusion is that bilayer splitting is considerably renormalized from the value obtained from band structure calculations. It would be extremely interesting to perform these experiments for higher values of doping. We roughly expect the splitting of the frequencies to increase with doping, but the full picture may be more complex because the density wave order parameter is also expected to decrease with doping, vanishing around the middle of the superconducting dome.

[1] Author to whom any correspondence should be addressed.

Contents

1. Introduction

The surprising quantum oscillations (QOs) in both hole- [1]–[11] and electron-doped cuprates [12] have raised an important question concerning the ground state of high-temperature superconductors [13]. Applied magnetic field between 35 and 85 T has been argued to quench the superconducting fluctuations, at least to a large degree, revealing the normal state. This is not surprising in electron-doped $Nd_{2-x}Ce_xCuO_4$ (NCCO), where the upper critical field H_{c2} is less than 10 T, but is somewhat surprising in hole-doped cuprates, where H_{c2} is extrapolated to be of the order of 100 T or greater [14]. One of the striking recent findings is the observation of multiple QO frequencies [7, 15]. To understand QO in hole-doped $YBa_2Cu_3O_{6+\delta}$ (YBCO) and stoichiometric $YBa_2Cu_4O_8$ (Y124), we shall follow a reasoning based on broken translational symmetry with perhaps an unconventional order parameter, $d_{x^2-y^2}$-density wave (DDW) [16]. The observed multiple frequencies should impose constraints not only on the theoretical models but also on interpretation of experiments. In some respects, similar results can be obtained within a mean field approximation using a spin density wave (SDW) theory, but we favor singlet DDW for numerous reasons discussed elsewhere [17]. More importantly, the quasiparticles of a singlet DDW have charge-e, spin-1/2 and a g-factor renormalized by residual Fermi liquid corrections. In the simplest treatment given here, we set $g = 2$. This characterization of the quasiparticles is consistent with a very recent measurement and its precise analysis [15], and perhaps eliminates any triplet order parameter, such as SDW or triplet DDW.

The experiments involving multiple QO frequencies not only indicate formation of Landau levels signifying finite quasiparticle residues even in underdoped cuprates, but also indicate coherent electron motion along the direction perpendicular to the CuO-plane. A bilayer Hamiltonian corresponding to YBCO was first written down in a paper in which an interlayer tunneling theory of superconductivity was proposed [18]. This Hamiltonian was subsequently derived from a downfolding process in a band structure calculation [19]. As long as the fermionic quasiparticles exist as excitations of the normal ground state, it is impossible to deny the existence of bilayer splitting, which results from the superposition of the electronic states

of the layers within a bilayer block. For each value of momentum, there is a bonding and an antibonding state that are split in energy. In the original context [18], it was argued that only in a superconducting state is such a coherent linear superposition possible. However, it is clear that the only requirement is the existence of a finite quasiparticle residue. An important effect discussed earlier [17] is that the phase of the DDW order parameter of the two layers within a bilayer block make a large difference. Even though the bilayer splitting can be substantial, the splitting of the Fermi surface areas for the out-of-phase case can be very small as compared to the in-phase case. We shall focus on these two alternatives amongst other considerations.

For many years it has been argued that the normal state of high-temperature superconductors is incoherent, especially in the underdoped regime. Here we shall focus on very low temperatures, where a sharp statement can be made. The view that the normal state is a non-Fermi liquid appears to be at variance with the striking QO experiments mentioned above. We look for consistency with recent experiments [7, 15] involving multiple frequencies, emphasizing, of course, the general aspects of a mean field theory. A further motivation is a measurement in a tilted magnetic field [20], where inconsistency of a scenario in which observed multiple frequencies arise from bilayer-split pockets is pointed out.

We emphasize a commensurate density wave order as the cause of Fermi surface reconstruction as revealed in QO measurements, although some evidence for incommensuration does exist [4]. The pressing questions can hopefully be addressed in a simpler setting. Why should the Fermi liquid picture be valid for the normal state? Is the motion along the direction perpendicular to the CuO-planes (c-axis) coherent? Why do other experimental probes of the electronic structure paint a very different picture of the fermiology? In reality, no direct evidence for any kind of long-range density wave order exists in the regime of interest to the QO measurements. Fluctuating order does not solve this dilemma, especially because the QO measurements require very large correlation lengths and nearly static order. The simplest possible explanation of the main aspects of the measurements call for long-range order. Moreover, there are strong arguments from detailed fits to the measurements that the relatively high magnetic field is not the root of these observations [11], beyond the obvious effect of suppressing superconductivity. Indeed, previous NMR measurements in Y124 up to at least 23.2 T have shown no signatures of field-induced order. Yet the QO measurements for this stoichiometric material are clear and unambiguous. Of course, NMR measurements [21] in higher fields of the order of 45 T would be interesting. Given these larger issues and many others, it is not particularly attractive to focus on details such as incommensurate versus commensurate order. In any case, it was shown previously [17] that within mean field theory it is quite simple to incorporate incommensurate order with very little change of the big picture; to go beyond mean field theory is quite difficult and is not particularly fruitful without sufficiently strong motivation. An important point with regard to DDW is that it is hidden from most common probes and its existence perhaps could have gone unnoticed.

The present paper is organized as follows. In section 2, we set up the effective Hamiltonian then discuss bilayer splitting in section 3. In section 4, we discuss our results in a perpendicular magnetic field and, in section 5, those in a tilted field. In section 6, we discuss how variation of parameters provides contrasting evidence of the out-of-phase versus in-phase DDW order. In section 7, we discuss in detail the temperature dependences and the oscillation magnitudes of both the magnetization and the specific heat within the Lifshitz–Kosevich–Luttinger formula but with Dingle factors reflecting vortex scattering rate in the mixed state. Section 8 contains remarks regarding unresolved puzzles.

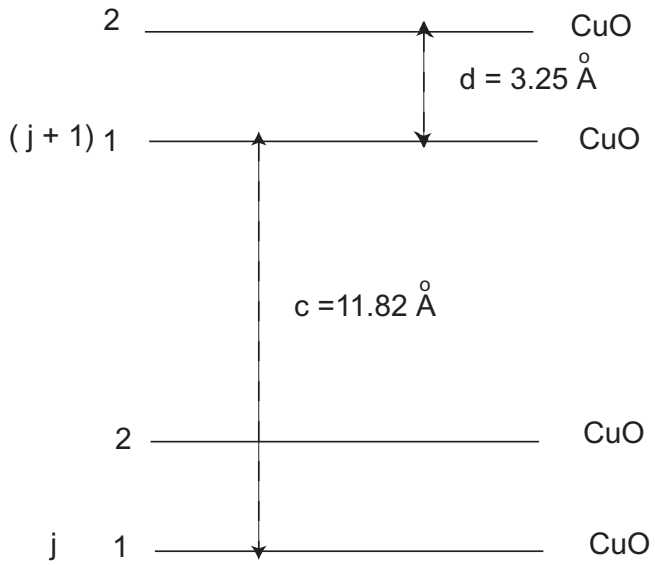

Figure 1. Bilayer structure of YBCO. Each unit cell contains a bilayer CuO block. Note that tunneling matrix elements within a bilayer unit and between the nearest-neighbor planes between the unit cells are kept; other matrix elements are exponentially smaller.

2. Hamiltonian

We consider a tight-binding Hamiltonian, H_0, which captures correctly the bilayer splitting and the matrix elements between the unit cells (see figure 1),

$$H_0 = \sum_{j,\mathbf{k}} \sum_{n=1}^{2} \epsilon(\mathbf{k}) c^{\dagger}_{n,j}(\mathbf{k}) c_{n,j}(\mathbf{k}) - \sum_{j,\mathbf{k}} t_{\perp}(\mathbf{k}) c^{\dagger}_{1,j}(\mathbf{k}) c_{2,j}(\mathbf{k}) + \text{h.c.}$$
$$- t_{\text{c}} \sum_{j,\mathbf{k}} c^{\dagger}_{1,j+1}(\mathbf{k}) c_{2,j}(\mathbf{k}) + \text{h.c.} \tag{1}$$

The fermion annihilation operator $c_{n,j}(\mathbf{k})$ depends on the bilayer index n within the unit cell and the index j refers to the unit cell. The spin indices are suppressed and $\mathbf{k} = (k_x, k_y)$ is a two-dimensional (2D) vector. Only the hopping matrix element, t_{c}, between the nearest-neighbor planes of two adjacent unit cells is kept, as the tunneling matrix elements to further neighbor planes are considerably smaller. For simplicity, t_{c} is assumed to be momentum independent, as very little is known about its precise form. This assumption will have little effect on our analysis. The bilayer matrix element corresponding to YBCO is [18]

$$t_{\perp}(\mathbf{k}) = \frac{t_{\perp}}{4} \left[\cos(k_x a) - \cos(k_y a)\right]^2, \tag{2}$$

where a is the in-plane lattice constant, ignoring slight orthorhombicity. H_0 can be further simplified by the canonical transformation [22],

$$c_n(\mathbf{k}, k_z) = \frac{1}{\sqrt{M}} \sum_j c_{n,j}(\mathbf{k}) \mathrm{e}^{\mathrm{i}k_z[jc+(n-1)d]} \mathrm{e}^{\mp \mathrm{i}\phi(k_z)/2}, \tag{3}$$

which diagonalizes it in the momentum space. Note the additional phase factors, $e^{-i\phi(k_z)}$ for $n=1$ and $e^{+i\phi(k_z)}$ for $n=2$. The choice of the phase $\phi(k_z) = -k_z d$ preserves the fermion anticommutaion rules and results in an energy spectrum that is periodic in $2\pi/c$, which preserves the periodicity of the conventional unit cell. The 2×2 bilayer block is still not diagonal and must be diagonalized further to obtain the quasiparticle dispersion. Note that t_c is a matrix element between the nearest-neighbor planes of the two bilayer blocks and will be chosen to be an adjustable parameter. The canonical transformation leads to

$$H_0 = \sum_{k_z,\mathbf{k}} \left\{ \sum_{n=1}^{2} \epsilon_{\mathbf{k}} c_n^\dagger(k_z,\mathbf{k}) c_n(k_z,\mathbf{k}) - [t_\perp(\mathbf{k}) + t_c e^{-ik_z c}] c_1^\dagger(k_z,\mathbf{k}) c_2(k_z,\mathbf{k}) + \text{h.c.} \right\}. \tag{4}$$

We use a common band structure [19, 23],

$$\epsilon_{\mathbf{k}} = -2t(\cos k_x a + \cos k_y a) + 4t' \cos k_x a \cos k_y a - 2t''(\cos 2k_x a + \cos 2k_y a), \tag{5}$$

with $t' = 0.32t$ and $t'' = \frac{1}{2}t'$, but t is chosen to be $t \approx 0.1$ eV. This renormalized value of t, as compared to the band structure value of 0.38 eV, seems to be phenomenologically more appropriate in the underdoped regime of interest to us. However, the specific results pertaining to the ground state at $T=0$ are independent of the magnitude of t; even if we had chosen $t = 0.38$ eV, the results would have been the same provided the remaining parameters are chosen proportionately. This is no longer true when we consider the $T \neq 0$ properties discussed in section 6. We shall first choose $t_\perp = 0.05t$ and $t_c = 0.013t$; these parameters are expected to be highly renormalized in the underdoped regime. Even when bilayer splitting is clearly observed in angle-resolved photoemission spectroscopy (ARPES) in heavily overdoped $Bi_2Sr_2CaCu_2O_{8+\delta}$ (Bi2212) [24], the actual magnitude of $t_\perp$ is severely overestimated by the band structure calculations, 300 meV, as opposed to the observed 88 meV. In the underdoped regime, the band structure value is likely to be more unreliable because of strong correlation effects. In section 6, we shall see how the variation of $t_\perp$ affects the principal conclusions.

The 2×2 Hamiltonian has the eigenvalues

$$\lambda_\pm(k_z,\mathbf{k}) = \epsilon_{\mathbf{k}} \pm \sqrt{t_c^2 + t_\perp(\mathbf{k})^2 + 2t_c t_\perp(\mathbf{k}) \cos k_z c}\,. \tag{6}$$

It is interesting to note that with our choice of the phase of the fermion operators, the distance between the layers in a bilayer block, d, does not appear explicitly in the spectrum, but only implicitly in the magnitude of the hopping matrix elements. The above result is very different from the conventional warping of layered materials that contain only one electronically active plane per unit cell, which leads to a dispersion $\epsilon_{\mathbf{k}} - 2t_c \cos k_z c$. Also, note that the interbilayer term is modulated by $t_\perp(\mathbf{k})$; see figure 2. As long as t_c is non-zero, the splitting at the nodal locations $(\pi/2a, \pi/2a)$ is non-zero. We now fold the Brillouin zone to the reduced Brillouin zone (RBZ) bounded by $k_y \pm k_x = \pm\pi/a$, corresponding to the twofold commensurate singlet DDW order parameter, and augment H_0 by H',

$$H' = \sum_{k_z,\mathbf{k}\in\text{RBZ}} \left[i\, W_{\mathbf{k}} c_1(k_z,\mathbf{k})^\dagger c_1(k_z,\mathbf{k}+\mathbf{Q}) + \text{h.c.} \right] + (1 \to 2), \tag{7}$$

where $\mathbf{Q} = (\pi/a, \pi/a)$ and the DDW gap $W_{\mathbf{k}}$ is real and is given by

$$W_{\mathbf{k}} = \frac{W_0}{2}(\cos k_x a - \cos k_y a). \tag{8}$$

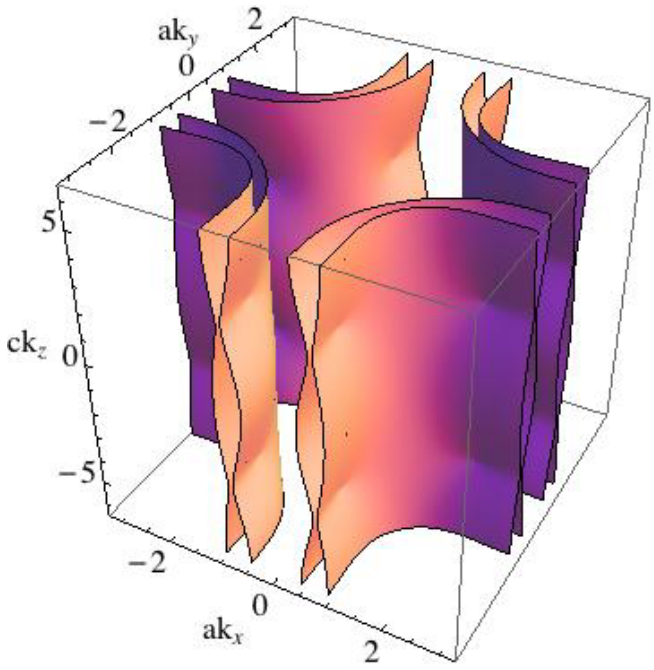

Figure 2. A greatly exaggerated illustration of warping of the bilayer split bands plotted in the extended zone $-2\pi \leqslant k_z c \leqslant 2\pi$, $-\pi \leqslant k_x a \leqslant \pi$ and $-\pi \leqslant k_y a \leqslant \pi$.

Note that the DDW order parameters are chosen to be in-phase for the layers. To reproduce the experimental frequencies, we require a somewhat large value of $W_0 = 0.85t$ within our mean field approximation; in section 6, we shall consider a small variation of this parameter.

The singlet DDW condensate is defined by [25]

$$\langle c^{\dagger}_{n',\sigma'}(\mathbf{k}', k_z) c_{n,\sigma}(\mathbf{k}, k_z)\rangle = \mathrm{i} W_{\mathbf{k}}\, \delta_{\sigma',\sigma}\delta_{n',n}\delta_{\mathbf{k}',\mathbf{k}+\mathbf{Q}}. \tag{9}$$

Note that it involves $\delta_{\sigma',\sigma}$ for spin indices. This is the reason why the spin indices can be conveniently suppressed. This is a particle–hole condensate that breaks the following symmetries: translation by a lattice spacing, time reversal, parity and a rotation by $\pi/2$, while the product of any two are preserved. The order parameter corresponds to angular momentum $\ell = 2$. Since there is no exchange symmetry between a particle and a hole, the orbital wave function does not constrain the spin wave function. Therefore, there is also a corresponding triplet DDW, which consists of a staggered pattern of circulating spin currents [25], as opposed to a staggered pattern circulating charge currents. In the present work, we shall consider only the singlet DDW order and make only brief remarks regarding the triplet DDW at the very end. The staggering is determined by the wave vector $\mathbf{Q}$.

3. Bilayer splitting

The combined Hamiltonian $H_0 + H'$ can be written in terms of the four-component spinor $\Psi^{\dagger}(\mathbf{k}, k_z) = \{c^{\dagger}_1(\mathbf{k}, k_z), c^{\dagger}_1(\mathbf{k}+\mathbf{Q}, k_z), c^{\dagger}_2(\mathbf{k}, k_z), c^{\dagger}_2(\mathbf{k}+\mathbf{Q}, k_z)\}$, suppressing once again the spin indices, which is irrelevant for a singlet DDW order parameter. In terms of this spinor, the

combined Hamiltonian is

$$\mathbb{H} = \sum_{\mathbf{k}\in \mathrm{RBZ}, k_z} \Psi^{\dagger}(\mathbf{k}, k_z)\mathbb{A}\Psi(\mathbf{k}, k_z), \tag{10}$$

where

$$\mathbb{A} = \begin{pmatrix} \epsilon_{\mathbf{k}} & \mathrm{i}W_{\mathbf{k}} & -t_{\perp}(\mathbf{k}) - t_{\mathrm{c}}\,\mathrm{e}^{-\mathrm{i}ck_z} & 0 \\ -\mathrm{i}W_{\mathbf{k}} & \epsilon_{\mathbf{k}+\mathbf{Q}} & 0 & -t_{\perp}(\mathbf{k}) - t_{\mathrm{c}}\,\mathrm{e}^{-\mathrm{i}ck_z} \\ -t_{\perp}(\mathbf{k}) - t_{\mathrm{c}}\,\mathrm{e}^{\mathrm{i}ck_z} & 0 & \epsilon_{\mathbf{k}} & \mathrm{i}W_{\mathbf{k}} \\ 0 & -t_{\perp}(\mathbf{k}) - t_{\mathrm{c}}\,\mathrm{e}^{\mathrm{i}ck_z} & -\mathrm{i}W_{\mathbf{k}} & \epsilon_{\mathbf{k}+\mathbf{Q}} \end{pmatrix}. \tag{11}$$

Note that the DDW order parameters in the two 2×2 diagonal blocks are in phase. The in-phase DDW order parameter corresponds to 'ferromagnetically' aligned staggered circulating currents in the layers within a bilayer block. The four eigenvalues of the matrix $\mathbb{A}$ are

$$\lambda^{\mathrm{s}}_{1\pm}(\mathbf{k}) = \frac{\epsilon_{\mathbf{k}} + \epsilon_{\mathbf{k}+\mathbf{Q}}}{2} \pm \left| \sqrt{\left(\frac{\epsilon_{\mathbf{k}} - \epsilon_{\mathbf{k}+\mathbf{Q}}}{2}\right)^2 + W_{\mathbf{k}}^2} - \sqrt{t_{\mathrm{c}}^2 + t_{\perp}(\mathbf{k})^2 + 2t_{\mathrm{c}}t_{\perp}(\mathbf{k})\cos k_z c} \right|, \tag{12}$$

and

$$\lambda^{\mathrm{s}}_{2\pm}(\mathbf{k}) = \frac{\epsilon_{\mathbf{k}} + \epsilon_{\mathbf{k}+\mathbf{Q}}}{2} \pm \left(\sqrt{\left(\frac{\epsilon_{\mathbf{k}} - \epsilon_{\mathbf{k}+\mathbf{Q}}}{2}\right)^2 + W_{\mathbf{k}}^2} + \sqrt{t_{\mathrm{c}}^2 + t_{\perp}(\mathbf{k})^2 + 2t_{\mathrm{c}}t_{\perp}(\mathbf{k})\cos k_z c} \right). \tag{13}$$

For a particle–hole condensate, when measured from the chemical potential, the spectra are

$$E^{s}_{1\pm}(\mathbf{k}) = \lambda^{s}_{1,\pm}(\mathbf{k}) - \mu, \tag{14}$$

$$E^{s}_{2\pm}(\mathbf{k}) = \lambda^{s}_{2,\pm}(\mathbf{k}) - \mu, \tag{15}$$

because both $\epsilon(\mathbf{k})$ and $\epsilon(\mathbf{k}+\mathbf{Q})$ are equally shifted by μ. If, on the other hand, the staggered circulating currents are 'antiferromagnetically' aligned within a bilayer block [17], that is, $\mathrm{i}W_{\mathbf{k}}$ is replaced by $-\mathrm{i}W_{\mathbf{k}}$ in the lower 2×2 diagonal block (*out-of-phase*), the corresponding eigenvalues are

$$\lambda^{\mathrm{a}}_{1\pm}(\mathbf{k}) = \frac{\epsilon_{\mathbf{k}} + \epsilon_{\mathbf{k}+\mathbf{Q}}}{2} \pm \left\{ W_{\mathbf{k}}^2 + \left(\left| \frac{\epsilon_{\mathbf{k}} - \epsilon_{\mathbf{k}+\mathbf{Q}}}{2} \right| - \sqrt{t_{\mathrm{c}}^2 + t_{\perp}(\mathbf{k})^2 + 2t_{\mathrm{c}}t_{\perp}(\mathbf{k})\cos k_z c} \right)^2 \right\}^{1/2}, \tag{16}$$

and

$$\lambda^{\mathrm{a}}_{2\pm}(\mathbf{k}) = \frac{\epsilon_{\mathbf{k}} + \epsilon_{\mathbf{k}+\mathbf{Q}}}{2} \pm \left\{ W_{\mathbf{k}}^2 + \left(\left| \frac{\epsilon_{\mathbf{k}} - \epsilon_{\mathbf{k}+\mathbf{Q}}}{2} \right| + \sqrt{t_{\mathrm{c}}^2 + t_{\perp}(\mathbf{k})^2 + 2t_{\mathrm{c}}t_{\perp}(\mathbf{k})\cos k_z c} \right)^2 \right\}^{1/2}. \tag{17}$$

Once again, measured from μ, we have

$$E^{\mathrm{a}}_{1\pm}(\mathbf{k}) = \lambda^{\mathrm{a}}_{1,\pm}(\mathbf{k}) - \mu, \tag{18}$$

$$E^{\mathrm{a}}_{2\pm}(\mathbf{k}) = \lambda^{\mathrm{a}}_{2,\pm}(\mathbf{k}) - \mu. \tag{19}$$

The contour plots for the Fermi surfaces corresponding to $\lambda^{\mathrm{s}}_{1\pm}$ and $\lambda^{\mathrm{s}}_{2\pm}$ for $k_z = 0$ are shown in figure 3. It is clear that while the electron pockets are observably split, the splitting of the hole pockets is much smaller. The chemical potential, $\mu = -0.78t$, was adjusted to yield approximately 10.3% hole doping. For an identical set of parameters, the splitting for the out-of-phase eigenvalues, $\lambda^{\mathrm{a}}_{1\pm}$ and $\lambda^{\mathrm{a}}_{2\pm}$, is considerably smaller, as shown in figure 4. It would be incorrect, however, to infer that the splitting is exactly zero (see table 2 below). Note that the absolute value of t does not change the frequencies because $\epsilon_F(\mathbf{k}; \alpha t, \alpha t', \alpha t'', \alpha t_{\perp}, \alpha t_{\mathrm{c}}, \alpha W_0) = \alpha\epsilon_{\mathrm{F}}(\mathbf{k}; t, t', t'', t_{\perp}, t_{\mathrm{c}}, W_0)$, as long as we also let $\mu \to \alpha\mu$.

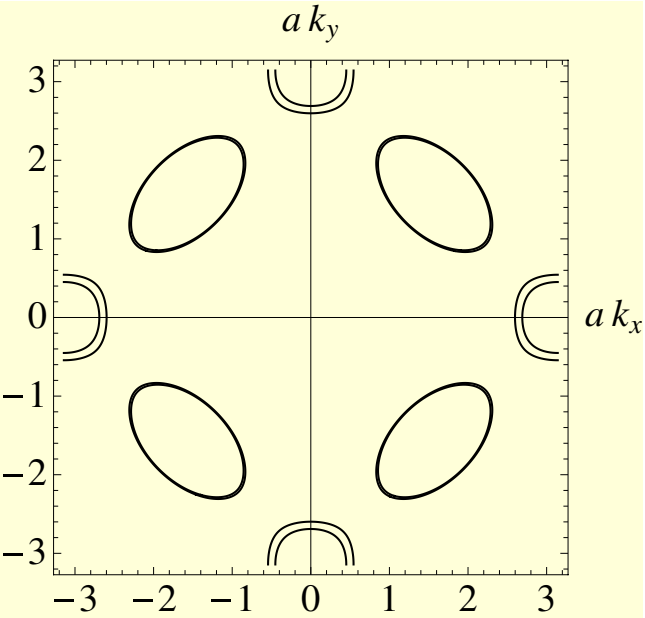

Figure 3. Bilayer splitting of the Fermi surfaces for the in-phase DDW order parameter. The cut is at $k_z = 0$, where the splitting is maximal. For clarity, the contours are plotted in the extended zone.

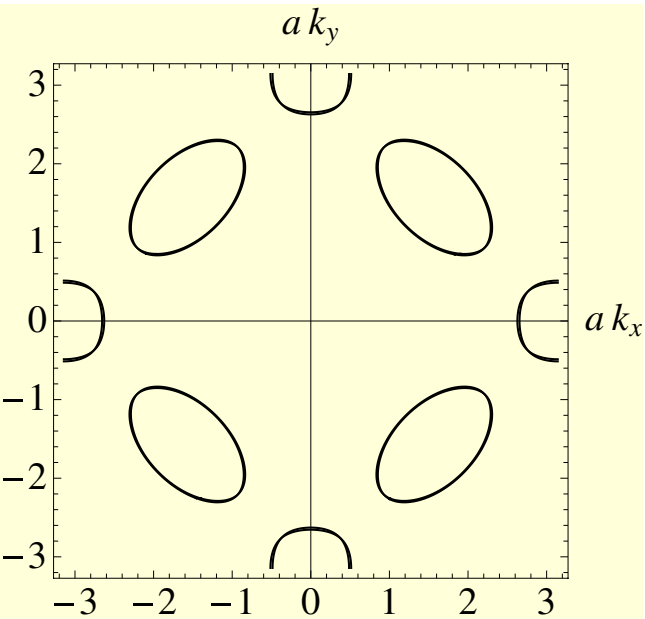

Figure 4. Bilayer splitting of the Fermi surfaces for the out-of-phase DDW order parameter. The cut is at $k_z = 0$. For clarity, the contours are plotted in the extended zone.

Table 1. Bilayer split frequencies for the in-phase DDW order. Here, $t_\perp = 0.05t$, $t_c = 0.013t$ and doping is approximately ∼10.3%. The band parameters are given in the text. The electron pocket is labeled as the e-pocket and the hole pocket as the h-pocket.

e-pocket ($k_z = 0$)	e-pocket ($k_z = \pi/c$)	h-pocket ($k_z = 0$)	h-pocket ($k_z = \pi/c$)
711 T	659 T	1051 T	1032 T
480 T	534 T	997 T	1015 T

4. Magnetic field perpendicular to the CuO-plane: the Onsager relation

QO frequencies can be obtained from the extremal areas, $\mathcal{A}(\epsilon_F)$, of the Fermi surface perpendicular to the applied magnetic field [26]. The Onsager relation for the frequency F is

$$F = \frac{\hbar c}{2\pi e}\mathcal{A}(\epsilon_F). \tag{20}$$

Of course, this formula presupposes that the quasiclassical approximation is valid and there are no significant magnetic breakdown effects.

Given the electronic structure, the doping dependence can be obtained from noting that there are two hole pockets within the RBZ and one electron pocket. These are further split by the bilayer coupling and warped by the k_z dependence. Taking into account two spin directions, the doping fraction of a given electron pocket corresponding to the bilayer bonding band b, x_e^b, is

$$x_e^b = 2\frac{2a^2c}{(2\pi)^3}\int_0^{\pi/a} dk_x \int_0^{\pi/a} dk_y \int_{-\pi/c}^{\pi/c} dk_z\, \theta\left(\mu - \epsilon^b(\mathbf{k}, k_z)\right). \tag{21}$$

There is an identical expression for the antibonding contribution x_e^a. Similarly, the two hole pockets contribute an amount x_h^b given by

$$x_h^b = 2\frac{2a^2c}{(2\pi)^3}\int_0^{\pi/a} dk_x \int_0^{\pi/a} dk_y \int_{-\pi/c}^{\pi/c} dk_z\, \theta\left(\epsilon^b(\mathbf{k}, k_z) - \mu\right), \tag{22}$$

with an identical antibonding contribution x_h^a. The total hole doping per CuO-plane is then

$$x_h = \tfrac{1}{2}(x_h^b + x_h^a - x_e^b - x_e^a). \tag{23}$$

The frequencies for the in-phase order parameter are given in table 1. The parameters were chosen, but not particularly optimized, to be similar to the observed frequencies [7] 540 ± 15, 630 ± 40, 450 ± 15 and 1130 ± 20 T. Out of four theoretically predicted frequencies corresponding to the electron pocket, only three are observed. The fourth observed frequency at 1130 T could correspond to the hole pocket that is split very little. Alternately, it may also be a harmonic. It has been a puzzle for some time [11], [27]–[31] as to why the hole pocket frequencies have such weak or non-existent signatures in QO measurements.

In contrast, the out-of-phase frequencies (table 2) do not resemble the experimental observations [7]. We provide an alternative picture in section 6 based on the experiment in [15]. Within the mean field approximation adopted here, it is not possible to distinguish between the in-phase and the out-of-phase cases [17] as far as the electronic energy is concerned. For this, one would need a detailed microscopic Hamiltonian. This is outside the scope of the present investigation. We therefore rely on experiments to distinguish between the two cases.

Table 2. Bilayer split frequencies for the out-of-phase DDW order. The parameters are the same as in table 1.

e-pocket ($k_z = 0$)	e-pocket ($k_z = \pi/c$)	h-pocket ($k_z = 0$)	h-pocket ($k_z = \pi/c$)
617 T	609 T	1044 T	1031 T
573 T	585 T	1002 T	1016 T

5. Tilted magnetic field

In this section, we calculate the effect of tilted magnetic field on QOs [32]. In figure 5 we show a cut of the Fermi surface with the plane $k_y = -\pi/a$. The intersection with the plane A is given by

$$\epsilon_{\mathrm{F}}\left(k_x, k_y, k_x \tan\varphi\right) = \mu. \tag{24}$$

If the Fermi surface does not depend on k_z, the area $\mathcal{A}_{\mathrm{O}}$ will be constant for all planes perpendicular to $k_z = 0$, and the area in the plane A will be given by $\mathcal{A}_A = \mathcal{A}_{\mathrm{O}}/\cos\varphi$ with a constant value of $\mathcal{A}_{\mathrm{O}}$. However, given the dependence on k_z, the area is

$$\mathcal{A}_A(\varphi)\cos\varphi = \int_{-\pi/a}^{-\pi/a} \mathrm{d}k_x \int_{-\pi/a}^{-\pi/a} \mathrm{d}k_y \theta\left[\epsilon_{\mathrm{F}}\left(k_x, k_y, k_x \tan\varphi\right) - \mu\right], \tag{25}$$

which can be computed numerically. The above result corresponds to $k_z = 0$. More generally, when the plane O is situated at an arbitrary value of k_z, we obtain

$$\mathcal{A}_A\left(k_z, \varphi\right)\cos\varphi = \int_{-\pi/a}^{-\pi/a} \mathrm{d}k_x \int_{-\pi/a}^{-\pi/a} \mathrm{d}k_y \theta\left[\epsilon_{\mathrm{F}}\left(k_x, k_y, k_z + k_x \tan\varphi\right) - \mu\right]. \tag{26}$$

Note that equation (26) is valid for angles $\varphi \leqslant \varphi_{\max}$ such that

$$\tan\varphi_{\max} = \frac{\pi/c}{\pi/a} = \frac{a}{c}. \tag{27}$$

Beyond this maximum angle, there are discontinuous jumps, and we do not attempt to treat this case. For hole pockets, the frequencies are summarized in figure 6. Similarly, for the electron pockets, the frequencies are shown in figure 7. Note that the vertical scales are different in figures 6 and 7. However, in this calculation we assumed that the extremal areas are centered at $k_x = k_y = k_z = 0$ and $k_x = k_y = 0$, $k_z = \pi/c$. This need not be the case in actual experiments and therefore a direct comparison with experiments is not possible. Finding the extremal areas with proper account of both bilayer splitting and warping is very complex, given the energy eigenvalues in equations (12) and (13). The calculation presented above is merely indicative of the trend of the frequencies as the tilting takes place.

It is also interesting to note how the frequencies are sequentially split as we first turn on $t_\perp$ and then t_{c}, which is shown in figure 8 for the magnetic field in the direction k_z. In figure 9, we illustrate the warping along k_z for an electron pocket. We represent a cut for $k_x = 0$ that yields $k_y a$ around 2.64. The vertical line at the center corresponds to a model where $t_\perp = t_{\mathrm{c}} = 0$. The two vertical lines at the left and right of the figure show the splitting when $t_\perp \neq 0$. The line on the left corresponds to the outer pocket and the line on the right to the inner pocket. As we turn on t_{c}, the warping is seen as two curved lines. It is clear that the warping has opposite sense for

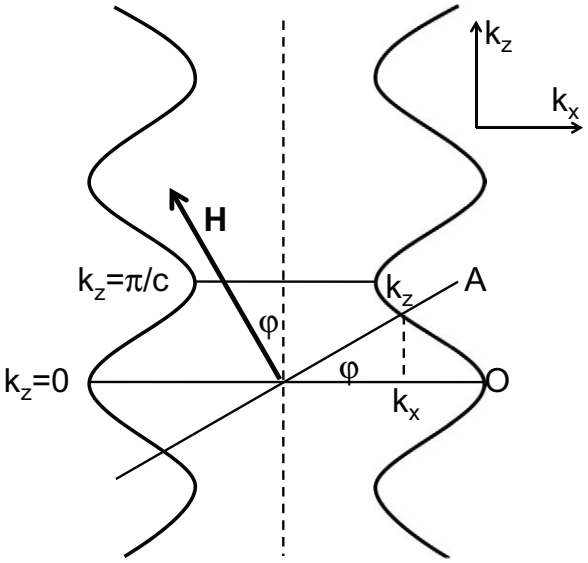

Figure 5. A cut of the Fermi surface of a pocket by a plane $k_y = -\pi/a$. **B** is the applied magnetic tilted at an angle φ.

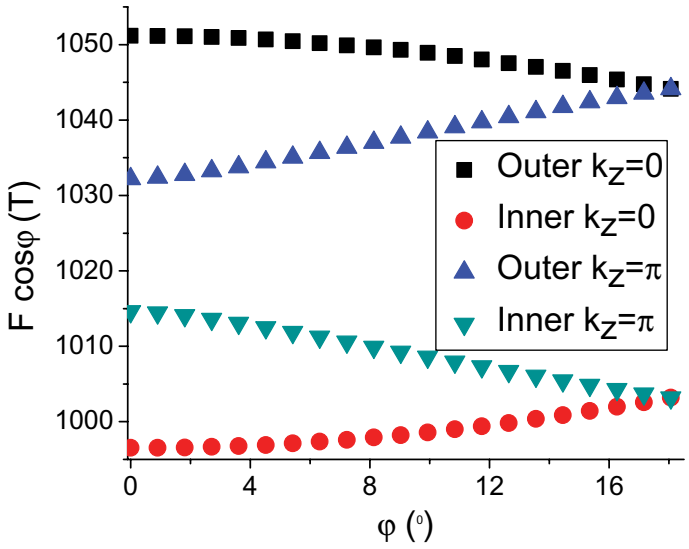

Figure 6. Hole pocket frequencies as a function of the tilt angle φ.

the outer and inner pockets. The bilayer splitting can be seen from the displacement of the left line by 0.0334 from the central line, while the right line is displaced by 0.0379 in the opposite direction. The splitting induced by $t_\perp$ is therefore not symmetric. To calculate the warping we can compute the distance between the lines at $k_z = 0$, obtaining 0.009 37 for the outer pocket and 0.0119 for the inner one. At $k_z = \pm\pi/c$, 0.009 58 is the displacement for the outer pocket and 0.011 58 is the displacement for the inner one. These numbers encode two important facts: firstly, the warping is different for the inner and the outer pockets and, secondly, it cannot be modeled with a simple cosine dependence.

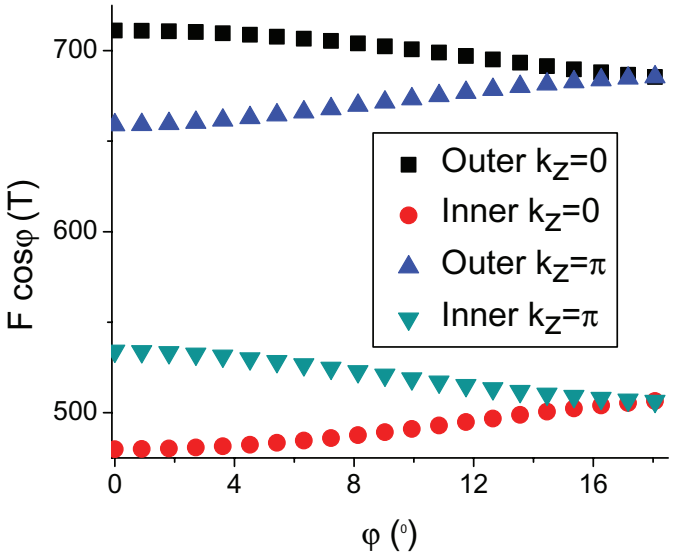

Figure 7. Electron pocket frequencies as a function of the tilt angle φ.

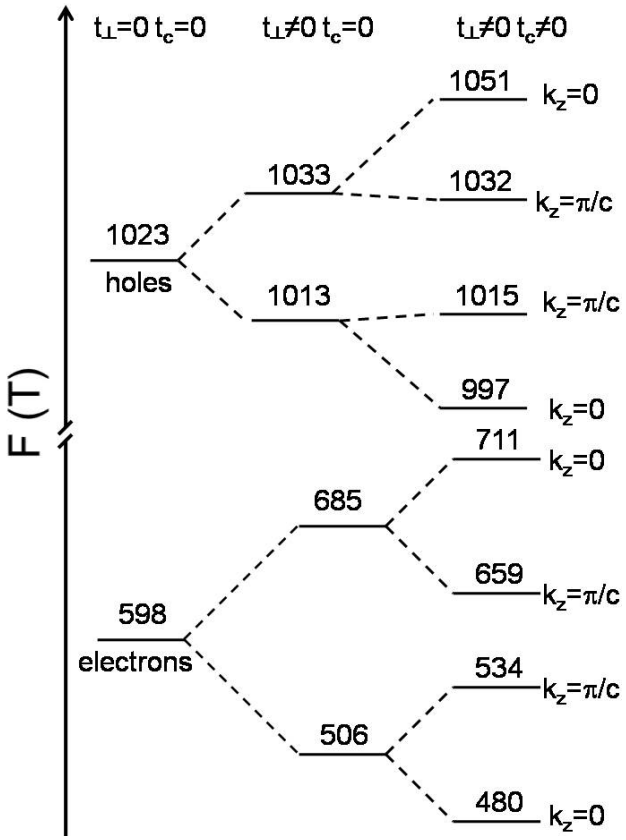

Figure 8. The hierarchy of frequency splitting for the in-phase DDW order parameter with the magnetic field normal to the CuO-plane, as we sequentially turn on $t_\perp$ and t_c. Not to scale.

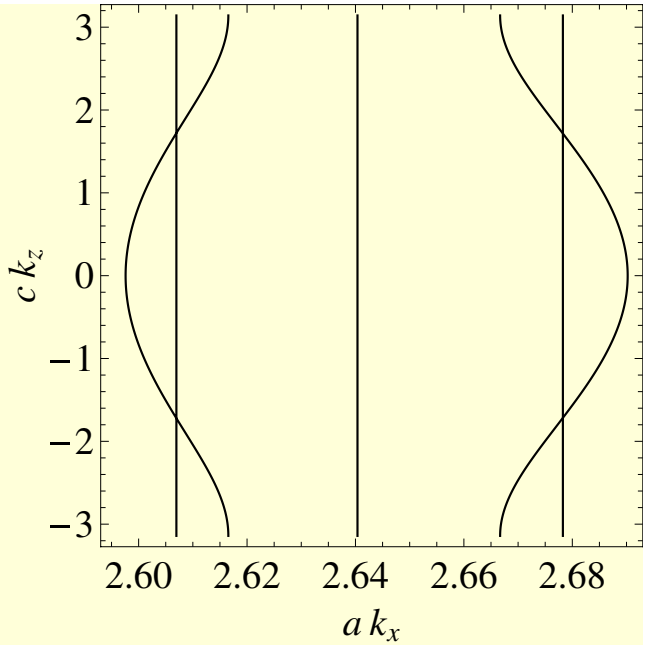

Figure 9. Warping of the bilayer split electron pockets.

6. Variation of parameters

Here we vary the parameters to see how the results change. The focus is the difference between the out-of-phase and the in-phase DDW order parameters. We have already seen that there is a qualitative distinction between them. However, given the recent measurements [15], we would like to see if one or the other can be made more consistent with these experiments. We stress that the phenomenological nature of our work precludes us from fitting parameters with certainty, nor is it our intention. We only look for some qualitative insights. However, since in this section we shall be computing the oscillatory part of the thermodynamic potential, as a function of temperature and magnetic field, not just the frequencies, a good estimate of the leading tight-binding matrix element t is necessary for materials relevant for QO experiments. Since there are no reliable ARPES for YBCO, the next best we can do is to rely on the recent tight-binding fit to the measured ARPES in Y124 [33], a system in which good QOs have been observed. Except for t, the ratios of the remaining band parameters to t are not very different from the band structure results given below equation (4). Thus, we simply take over the value of t determined from ARPES in Y124, which is $t = 0.154$ eV (the average of the fit to the bonding and antibonding bands). Additionally, we would like to see if one can tolerate a much larger value of bilayer matrix element, $t_\perp$, as compared to the earlier section and still find consistency with experiments. We shall see that this is indeed possible, but only for the out-of-phase DDW order parameter.

In this section, we keep all the band structure parameters fixed, including t_c, but more than double the bilayer matrix element to $t_\perp = 0.12t = 0.0185$ eV, resulting in a splitting of 37 meV, which is reasonable compared to the overdoped Bi2212, where it is measured to be 88 meV; one expects renormalization with underdoping. To keep the doping level more or less fixed ($\approx$10.7%), we set $\mu = -0.775t$ and $W_0 = 0.9t$. The resulting oscillation frequencies are shown

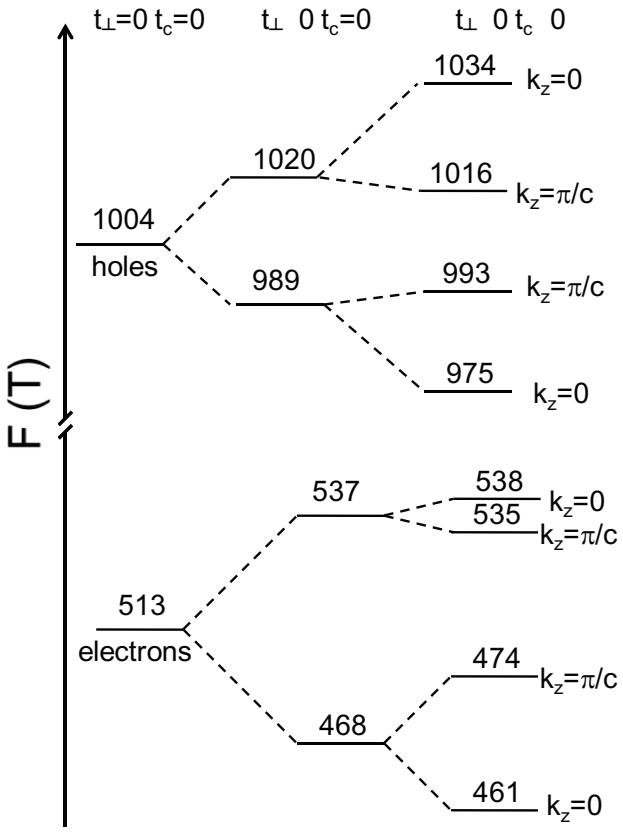

Figure 10. The hierarchy of frequency splitting for the out-of-phase DDW order parameter with the magnetic field normal to the CuO-plane, as we sequentially turn on $t_\perp$ and t_c. Not to scale.

Table 3. Bilayer split frequencies for the out-of-phase DDW order parameter. Here, $t_\perp = 0.12t$ and doping is ≈10.7%. The band structure parameters, t' and t'', are unchanged, $t' = 0.32t$ and $t'' = 0.5t'$, but $W_0 = 0.9t$, where $t = 0.154$ eV.

e-pocket ($k_z = 0$)	e-pocket ($k_z = \pi/c$)	h-pocket ($k_z = 0$)	h-pocket ($k_z = \pi/c$)
538 T	535 T	1034 T	1015 T
461 T	474 T	975 T	993 T

in table 3, and the Fermi surfaces at $k_z = 0$ are plotted in figure 11. The two groups of electron pocket frequencies are close to each other and so are the two groups of hole pocket frequencies, despite much larger bilayer splitting. The warping of the outer electron pocket is only 3 T and that of the inner pocket is 13 T. It is even possible to tolerate larger $t_\perp$, but we have not explored it further. It is again useful to examine the frequency diagram. This is shown in figure 10 and is quite different from figure 8.

In contrast, for the same set of parameters as above, the in-phase DDW results in frequencies that are no longer close to the recent experiments [15], as shown in table 4. The warping of the outer electron pocket is 51 T and that of the inner electron pocket is 57 T.

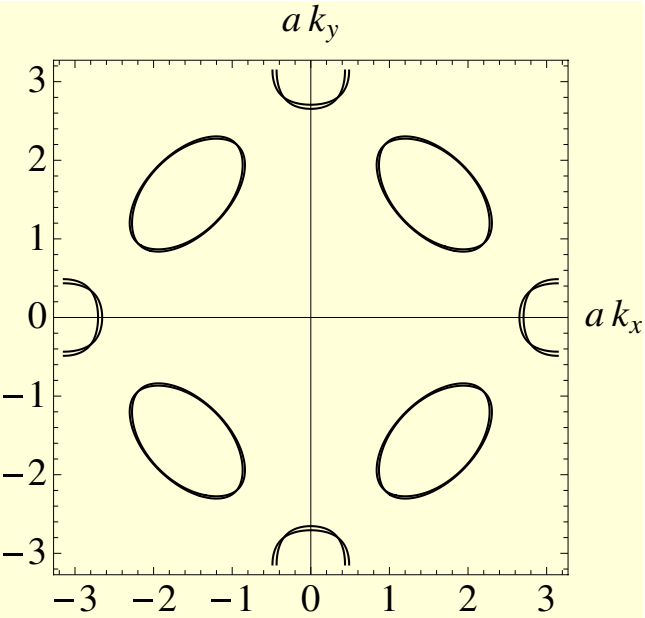

Figure 11. Bilayer splitting for the out-of-phase DDW order parameter. The cut is at $k_z = 0$. For clarity, the contours are plotted in the extended zone. Here, $t_\perp = 0.12t$ and doping is ≈10.7%. The band structure parameters, t' and t'', are unchanged, $t' = 0.32t$ and $t'' = 0.5t'$, but $W_0 = 0.9t$, where $t = 0.154$ eV.

Table 4. Bilayer split frequencies for the in-phase DDW order parameter. Here, $t_\perp = 0.12t$ and doping is ≈10.7%. The band structure parameters are unchanged, $t' = 0.32t$ and $t'' = 0.5t'$, but $W_0 = 0.9t$, where $t = 0.154$ eV. Compare with table 3.

e-pocket ($k_z = 0$)	e-pocket ($k_z = \pi/c$)	h-pocket ($k_z = 0$)	h-pocket ($k_z = \pi/c$)
750 T	699 T	1046 T	1022 T
250 T	307 T	965 T	988 T

6.1. Cyclotron masses and the second derivatives of the extremal areas

In the following section, we shall need the cyclotron masses and the second derivatives of the extremal areas. These are calculated numerically and are summarized in tables 5 and 6. The second derivatives of the extremal areas with respect to k_z are more difficult to calculate. We fit the areas near $k_z = 0$ and $k_z = \pi/c$ by a fourth-order polynomial with only even terms (odd terms are zero within numerical precision)

$$\mathcal{A} \approx \mathcal{A}_0 + \frac{\mathcal{A}_2}{2}(k_z c)^2 + \frac{\mathcal{A}_4}{24}(k_z c)^4 \tag{28}$$

$$\mathcal{A} \approx \mathcal{A}_0 + \frac{\mathcal{A}_2}{2}\left[(k_z c) - \pi\right]^2 + \frac{\mathcal{A}_4}{24}\left[(k_z c) - \pi\right]^4. \tag{29}$$

It is interesting to note that while the cyclotron masses depend on the in-plane hopping matrix element t, the second derivatives of the extremal areas are independent of t.

Table 5. Cyclotron masses in units of the free electron mass for the out-of-phase DDW order parameter.

e-pocket ($k_z = 0$)	e-pocket ($k_z = \pi/c$)	h-pocket ($k_z = 0$)	h-pocket ($k_z = \pi/c$)
1.67	1.64	0.99	0.97
1.47	1.49	0.93	0.95

Table 6. The fitting coefficients of the extremal areas.

	$\mathcal{A}_0$	$\mathcal{A}_2$	$\mathcal{A}_4$
h-pocket ($k_z = 0$)	1.455 42	−0.008 04	−0.000 51
h-pocket ($k_z = 0$)	1.372 38	0.007 76	−0.004 88
e-pocket ($k_z = 0$)	0.756 96	−0.001 19	−0.003 05
e-pocket ($k_z = 0$)	0.649 28	0.009 02	−0.024 21
h-pocket ($k_z = \pi/c$)	1.430 00	0.041 16	−1.163 30
h-pocket ($k_z = \pi/c$)	1.397 61	−0.041 02	1.180 22
e-pocket ($k_z = \pi/c$)	0.753 15	0.002 69	−0.013 03
e-pocket ($k_z = \pi/c$)	0.667 71	−0.008 62	0.006 37

7. Oscillation amplitudes of specific heat and magnetization

Within the Fermi liquid theory, Luttinger [34] has shown that the thermodynamic potential is given by ($\beta = 1/k_B T$)

$$\Omega = -\frac{1}{\beta}\sum_r \ln\left[1 + e^{\beta(\mu - E_r)}\right], \tag{30}$$

where $\{E_r\}$ constitute the spectra of elementary excitations behaving like independent particles in a magnetic field, including Fermi liquid corrections; r denotes the collection of quantum numbers: the Landau level n, k_z and the spin σ. The spectra $\{E_r\}$ in a crystalline solid in high magnetic fields are, of course, not easy to calculate, especially if we have to include bilayer splitting and the DDW order discussed above, but a rigorous answer can be given within an asymptotic expansion. Luttinger has shown that the problem maps onto that solved by Lifshitz and Kosevich (LK) [35] in which the thermodynamic potential depends on the extremal areas of closed orbits, the derivative of the areas with respect to energy at the chemical potential, and the second derivative of the extremal areas with respect to k_z. The beauty of this approach is that it is not necessary to know E_r explicitly. Thus, even given the complexity of the present problem, the procedure to calculate the oscillatory part of the thermodynamic potential is straightforward. As with all asymptotic expansions, the validity of the procedure far surpasses what we may naively perceive to be the regime of validity. Thus the LK formula has stood the test of time, especially with Luttinger's Fermi liquid corrections.

For simplicity, in this section we shall consider magnetic field only in the c-direction. Taking into account only the fundamental frequencies, F_i, the oscillatory part of Ω is

$$\frac{\Omega}{V} \propto -H^{5/2}\sum_i \frac{1}{m_i^*}\left|\frac{\partial^2 S_i}{\partial k_z^2}\right|^{-1/2} \psi(\lambda_i)\cos\left[\frac{2\pi F_i}{H} \pm \frac{\pi}{4}\right]\cos\left(\pi\frac{m_i^*}{m}\right). \tag{31}$$

The phase $\pm\pi/4$ corresponds to positive or negative sign of the second derivative of the extremal area with respect to k_z. The sum is over all extremal surfaces, and m_i^* is the cyclotron effective mass given by (m is the free electron mass)

$$m_i^* = \frac{\hbar^2}{2\pi}\left|\frac{\partial S_i}{\partial \mu}\right|, \tag{32}$$

and $\left|\frac{\partial^2 S_i}{\partial k_z^2}\right|$ is the second derivative of the area of the Fermi surface with respect to k_z. The argument of the function

$$\psi\left(\lambda_i\right) = \frac{\lambda_i}{\sinh \lambda_i} \tag{33}$$

is

$$\lambda_i = \frac{2\pi^2 k_{\mathrm{B}} T}{\hbar \omega_{ci}^*}. \tag{34}$$

The cyclotron frequencies are given by $\omega_{ci}^* = eH/m_i^* c$. The oscillatory part of the specific heat is then

$$\frac{C_V^{\mathrm{osc}}}{V} \propto -T H^{1/2} \sum_i m_i^* \left|\frac{\partial^2 S_i}{\partial p_z^2}\right|^{-1/2} \psi''\left(\lambda_i\right) \cos\left[\frac{2\pi F_i}{H} \pm \frac{\pi}{4}\right] \cos\left(\pi \frac{m_i^*}{m}\right), \tag{35}$$

where $\psi''(\lambda)$ is the second derivative of $\psi(\lambda)$ with respect to λ. Similarly, the leading oscillatory term of the magnetization is

$$\frac{M}{V}^{\mathrm{osc}} \propto -H^{1/2} \sum_i \frac{F_i}{m_i^*} \left|\frac{\partial^2 S_i}{\partial p_z^2}\right|^{-1/2} \psi\left(\lambda_i\right) \cos\left[\frac{2\pi F_i}{H} \pm \frac{\pi}{4}\right] \cos\left(\pi \frac{m_i^*}{m}\right). \tag{36}$$

These results need to be supplemented by the Dingle factors that damp the oscillations due to scattering from defects or vortices in the vortex liquid state or both. We expect the total scattering rate to be given by the combination of defect and vortex scattering rates

$$\frac{\hbar}{\tau} = \frac{\hbar}{\tau_{\mathrm{d}}} + \frac{\hbar}{\tau_{\mathrm{v}}}. \tag{37}$$

Moreover, these scattering rates must depend on the particular extremal area, i, under consideration. The calculation of the Dingle factors

$$\mathcal{D}_i = \mathrm{e}^{-\pi/\omega_{ci}^* \tau_i}, \tag{38}$$

especially in the mixed phase including disorder, with coexisting fluctuating d-wave superconducting order parameter and DDW, is a daunting task. Previously, we have shown rigorously that almost any form of conventional disorder due to defects in a pure DDW state suppresses the electron pockets more than the hole pockets. For the vortex scattering rate, however, an approximate treatment based on a paper by Stephen [36] led to an interesting prediction relating the Dingle factors of electron and hole pockets (not including bilayer splitting) in the commensurate case, which is

$$\left(\frac{\hbar}{\omega_{\mathrm{c}} \tau_{\mathrm{v}}}\right)_{\mathrm{h}} \approx \sqrt{2} \left(\frac{\widetilde{m}}{m^*}\right)^{3/2} \left(\frac{\hbar}{\omega_{\mathrm{c}} \tau_{\mathrm{v}}}\right)_{\mathrm{e}}, \tag{39}$$

where $\widetilde{m}$ is a characteristic scale having the dimension of mass corresponding to the *massless* nodal fermions of the DDW (!), and m^* is the cyclotron mass corresponding to the electron

pocket, as defined above (note that the notations are different here from [29]), which in turn is very close to the band mass defined by expanding around the bottom of the electron pocket. Although the precise numerical relation is difficult to control, it is reasonable to set $\mathcal{D}_h = \mathcal{D}_e^{\alpha}$, with $\alpha = 1.5$–4.5 for phenomenological purposes; we had estimated this parameter earlier to be 4.4 [29].

7.1. Specific heat and magnetization

With the frequencies given in table 3, the cyclotron masses in table 4 and the second derivatives of the areas in table 5, we can compute the oscillatory parts of the specific heat and the magnetization provided we can make reasonable estimates of the Dingle factors. The Dingle factor for electrons is a bit more controlled because the band mass obtained by expanding around the antinodal points is quite consistent with the computed cyclotron masses. Assuming that samples have negligible disorder, we shall estimate the scattering rate of the electrons to be given by the vortex scattering rate, which, following an analysis of Stephen [36], was found to be [17, 29]

$$\left(\frac{1}{\tau_v}\right)_e = \frac{\Delta_0^2}{\hbar}\left(1 - \frac{H}{H_{c2}}\right)\sqrt{\frac{\pi}{|\mu|\hbar\omega_c}}, \tag{40}$$

where Δ_0 is the magnitude of the $T = 0$ superconducting gap, which we set to be $\approx$10 meV for the relevant doping range. The cyclotron frequency $\omega_c = eH/m^*c$, with m^* given in table 4. With the present set of parameters and with the average value of m^*, we find that

$$\left(\frac{1}{\tau_v}\right)_e \approx 8.5 \times 10^{12}\,\mathrm{s}^{-1}, \tag{41}$$

where we used, as a typical case, $H = 40\,\mathrm{T}$ and $H_{c2} \approx 100\,\mathrm{T}$. We believe that this gives the correct order of magnitude; for the earlier set of parameters we estimated it to be $3 \times 10^{12}\,\mathrm{s}^{-1}$ [17]. The Dingle factors of the holes are more complex [17, 29] because they have to be estimated taking into account the nodal fermions for DDW, but it is not unreasonable to assume $\alpha \approx 2$ in the relation $\mathcal{D}_h = \mathcal{D}_e^{\alpha}$ uniformly for all electron and hole pockets.

The computed specific heat at four representative temperatures is shown in figure 12. It is interesting to note that there is a π-phase shift from high to low temperatures. The same results are visualized in a 3D plot in figure 13. As a function of temperature and magnetic field the oscillations go through a node, which is also visible in figure 12. The reason for this is the factor $\psi''(\lambda)$ in the formula for the specific heat. The Fourier transform of the oscillations in $1/H$, on the other hand, shows a more complex structure for specific heat, as shown in figure 14, which, however, is very sensitive to the Dingle factor, the range of $1/H$ over which the Fourier transform is performed, and the windowing technique. The results shown here use no windowing technique, and the range of the magnetic field is $1/60 \leqslant 1/H \leqslant 1/20$. The non-monotonic behavior of the Fourier transform in figure 14 can be understood by glancing at figure 13. Because of the aforementioned node, the transition from 6 to 4 K lowers the amplitude. At 2 K, the amplitude recovers again and then finally decreases again at 1 K. Note that only one dominant frequency is seen.

Similarly, we also plot the oscillations of the magnetization as a function of $1/H$ in figure 15, but it is difficult to detect multiple frequencies with the naked eye. Even in the Fourier transform over a range $1/60 \leqslant 1/H \leqslant 1/20$, shown in figure 16, the multiple electron pocket frequencies known to be present in the formula are not resolved. The Fourier transform

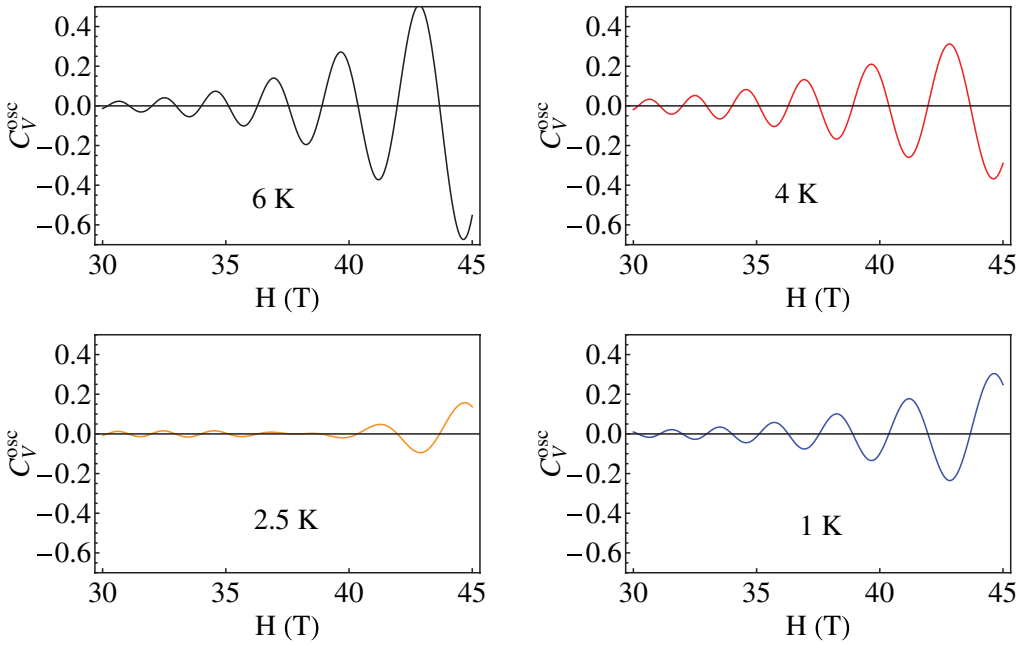

Figure 12. Oscillatory part of the specific heat as a function of the magnetic field at representative temperatures. Note the phase shift by π as the temperature is lowered. The vertical scale is in arbitrary units.

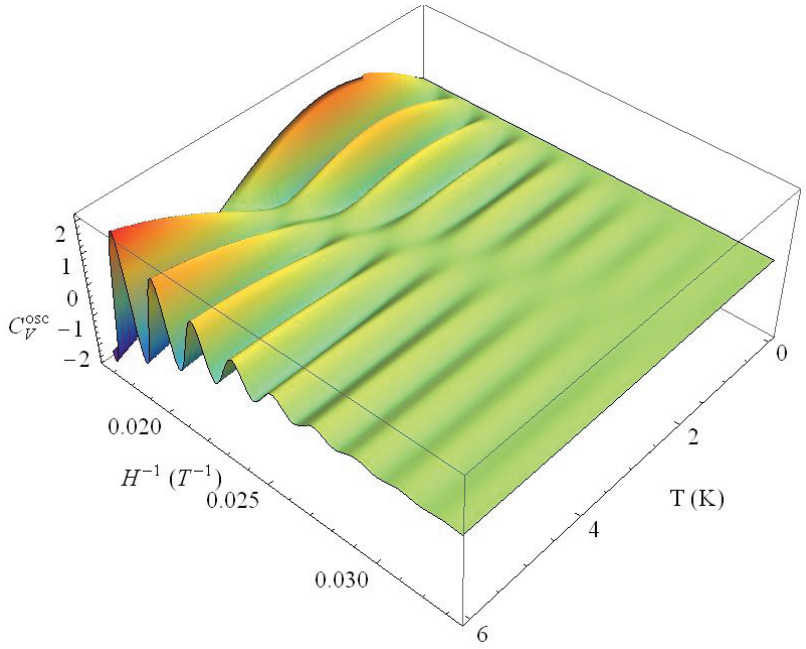

Figure 13. Oscillatory part of the specific heat as a function of temperature and the inverse of the magnetic field. Note the presence of nodes for intermediate values of the magnetic field and the temperature. The vertical scale is in arbitrary units.

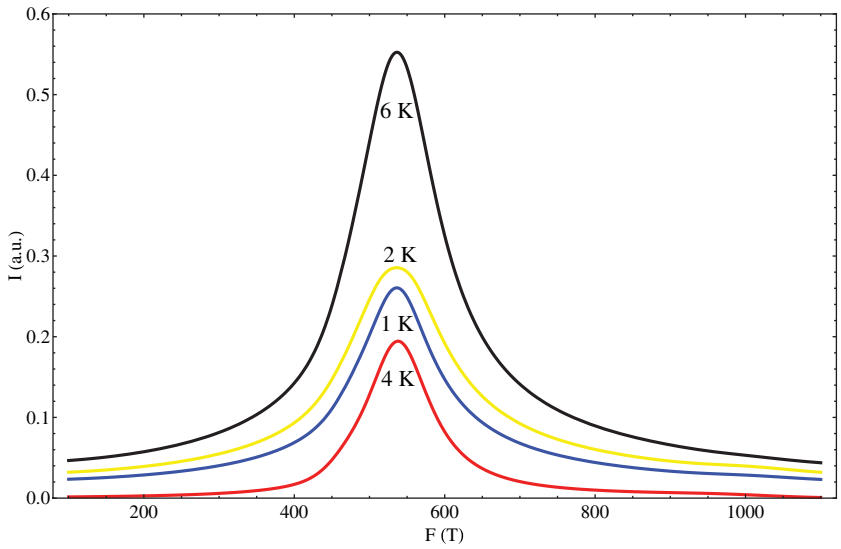

Figure 14. Absolute value of the Fourier transform, I, in arbitrary units of the oscillations of the specific heat as a function of the frequency F in units of Tesla. No windowing was performed, and the field range was $1/60 \leqslant 1/H \leqslant 1/20$.

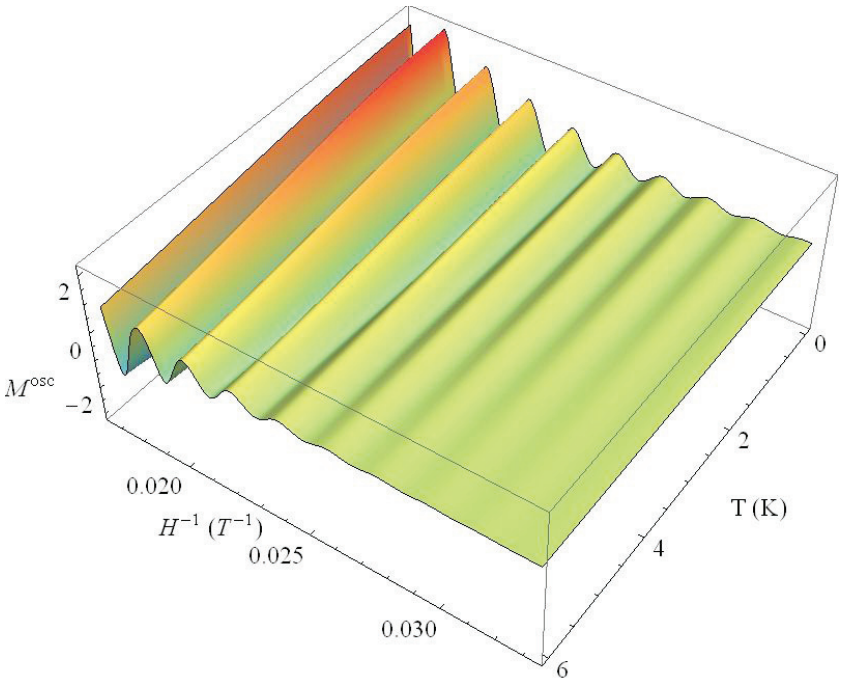

Figure 15. Oscillatory part of the magnetization as a function of temperature and the inverse of the magnetic field. There are no nodes at intermediate temperatures, as in the case of specific heat. The vertical scale is in arbitrary units.

is now monotonic as a function of temperature, unlike the results for the specific heat. The arrow indicates weak, unresolved hole pocket frequencies around 1000 T (see figure 10). The two electron pocket frequencies at 535 and 538 T strongly overlap and lead to a large amplitude.

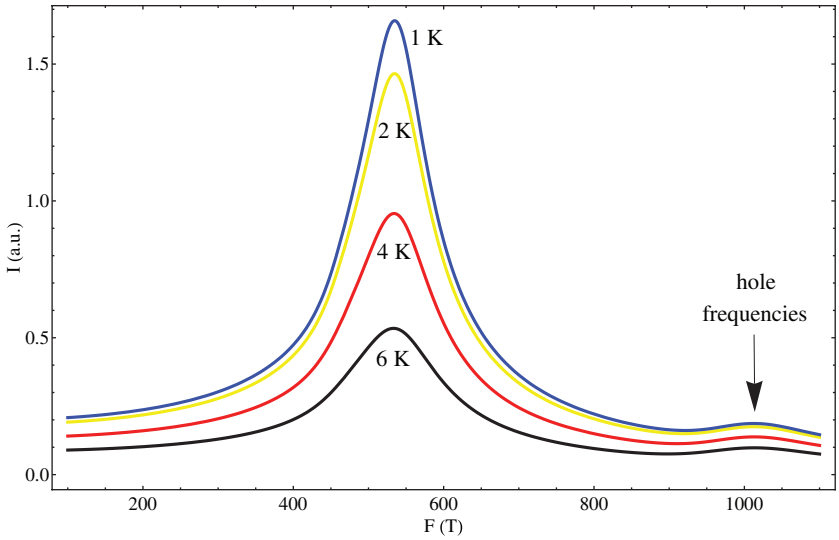

Figure 16. Absolute value of the Fourier transform, I, in arbitrary units of the oscillations of the magnetization as a function of the frequency F in units of Tesla with no windowing, and the field range of $1/60 \leqslant 1/H \leqslant 1/20$.

The spin interference factor $\cos(\pi m^*/m)$ plays an important role in the respective weights of the various frequencies.

8. Conclusion

We have argued that bilayer splitting and warping of the electronic dispersion in k_z are necessary consequences of a reconstructed Fermi liquid normal state, and measurements in a tilted magnetic field can be useful in probing the frequency spectra of QOs. The small value of the warping is intimately connected to the large ratio of the in-plane to c-axis resistivities. However, the magnitude of bilayer splitting necessary to produce overall consistency with experiments for the in-phase DDW order is strongly renormalized ($\sim$10 meV) from the band structure value ($\sim$300 meV). Note that the distance between the layers is only 3.25 Å, similar to the in-plane lattice constant. In contrast, with the out-of-phase DDW order, a larger value of bilayer splitting ($\sim$37 meV) can be tolerated. This is an important consequence of the out-of-phase DDW order. Although strong electronic correlations in the underdoped regime must be responsible for such renormalized parameters, a convincing explanation is missing despite many speculations, especially because the effective mass is only about twice the free electron mass. It would be interesting to carry out these QO measurements for larger hole-doping for which we generally expect the splitting to increase, unless some other effects involving the decrease in the magnitude of the order parameter intervenes. It is worth emphasizing once again that, even in heavily overdoped Bi2212, the renormalization of the observed bilayer splitting, 88 meV, in ARPES, as compared to the band structure value of 300 meV, is still not understood.

The calculations presented here can easily be extended within a mean field theory to SDW and incommensurate order along the lines discussed elsewhere [17]. A more illuminating exercise is to compare and contrast QOs in hole- and electron-doped cuprates [37]. The likely differences in the upper critical fields lead to important physical differences. Further work in this

direction is in progress. The triplet DDW [25] at the simplest mean field level produces results similar to SDW, which is also a triplet order parameter, but with orbital angular momentum zero. Such triplet order parameters are necessary to explain the experiments [6] involving the non-existence of spin zeros in QO. On the other hand, more recent experiments [15] have revealed spin zeros and have concluded that quasiparticles behave like charge-e, spin-1/2 fermions with a g-factor consistent with 2.2. This is strongly indicative of a singlet order parameter, but not a triplet order in the particle–hole channel, such as SDW or triplet DDW [38].

Although we have obtained consistency with experiments using the Fermi liquid theory, it is not certain whether non-Fermi liquid aspects should be ignored, at least insofar as underdoped YBCO is concerned. Convincing explanation of the lack of the hole pocket frequencies required by the Luttinger sum rule [39]–[41] and the inconsistency with Fermi arcs observed in ARPES, albeit in zero magnetic field, is missing. We know of one example, the $\nu = 1/2$ quantum Hall effect, which despite being a non-Fermi liquid has a phenomenology similar to a Fermi liquid in many respects [42]. The situation in NCCO is clearer [37], however. We hope that our work will shed light on these exciting sets of experimental developments.

Acknowledgments

We thank Cyril Proust for many interesting correspondences and S Sebastian for drawing our attention to the measurements in a tilted magnetic field. We are grateful to D Bonn and G Boebinger for sharing with us their unpublished data. We also thank E Abrahams for a critical reading of the manuscript. This work was supported by the NSF under grant no. DMR-0705092. DGA acknowledges financial support from Fundacion Cajamadrid through its grant program and from the Spanish MCInn through the research project ref. FIS2007-65702-C02-02.

References

[1] Doiron-Leyraud N, Proust C, LeBoeuf D, Levallois J, Bonnemaison J-B, Liang R, Bonn D A, Hardy W N and Taillefer L 2007 Quantum oscillations and the Fermi surface in an underdoped high-T_c superconductor *Nature* **447** 565–8

[2] Jaudet C *et al* 2008 de Haas–van Alphen oscillations in the underdoped high-temperature superconductor $YBa_2Cu_3O_{6.5}$ *Phys. Rev. Lett.* **100** 187005–4

[3] LeBoeuf D *et al* 2007 Electron pockets in the Fermi surface of hole-doped high-T_c superconductors *Nature* **450** 533–6

[4] Sebastian S E, Harrison N, Palm E, Murphy T P, Mielke C H, Liang R, Bonn D A, Hardy W N and Lonzarich G G 2008 A multi-component Fermi surface in the vortex state of an underdoped high-T_c superconductor *Nature* **454** 200–3

[5] Yelland E A, Singleton J, Mielke C H, Harrison N, Balakirev F F, Dabrowski B and Cooper J R 2008 Quantum oscillations in the underdoped cuprate $YBa_2Cu_4O_8$ *Phys. Rev. Lett.* **100** 047003–4

[6] Sebastian S E, Harrison N, Mielke C H, Liang R, Bonn D A, Hardy W N and Lonzarich G G 2009 Spin-order driven Fermi surface revealed by quantum oscillations in an underdoped high-T_c superconductor *Phys. Rev. Lett.* **103** 256405

[7] Audouard A, Jaudet C, Vignolles D, Liang R, Bonn D A, Hardy W N, Taillefer L and Proust C 2009 Multiple quantum oscillations in the de Haas–van Alphen spectra of the underdoped high-temperature superconductor $YBa_2Cu_3O_{6.5}$ *Phys. Rev. Lett.* **103** 157003

[8] Vignolle B, Carrington A, Cooper R A, French M M J, Mackenzie A P, Jaudet C, Vignolles D, Proust C and Hussey N E 2008 Quantum oscillations in an overdoped high-T_c superconductor *Nature* **455** 952–5

[9] Bangura A F *et al* 2008 Small Fermi surface pockets in underdoped high temperature superconductors: observation of Shubnikov–de Haas oscillations in $YBa_2Cu_4O_8$ *Phys. Rev. Lett.* **100** 047004–4
[10] Singleton J *et al* 2010 Magnetic quantum oscillations in $YBa_2Cu_3O_{6.61}$ and $YBa_2Cu_3O_{6.69}$ in fields of up to 85 T; patching the hole in the roof of the superconducting dome *Phys. Rev. Lett.* **104** 086403
[11] Rourke P M C, Bangura A F, Proust C, Levallois J, Doiron-Leyraud N, LeBoeuf D, Taillefer L, Adachi S, Sutherland M L and Hussey N E 2010 Fermi surface reconstruction and two-carrier modeling of the Hall effect in YBa_2Cu_4O8 *Phys. Rev.* B **82** 020514
[12] Helm T, Kartsovnik M V, Bartkowiak M, Bittner N, Lambacher M, Erb A, Wosnitza J and Gross R 2009 Evolution of the Fermi surface of the electron-doped high-temperature superconductor $Nd_{2-x}Ce_xCuO_4$ revealed by Shubnikov–de Haas oscillations *Phys. Rev. Lett.* **103** 157002–4
[13] Chakravarty S 2008 Physics—from complexity to simplicity *Science* **319** 735–6
[14] Li L, Wang Y, Naughton M J, Komiya S, Ono S, Ando Y and Ong N P 2007 Magnetization, Nernst effect and vorticity in the cuprates *J. Magn. Magn. Mater.* **310** 460–6
[15] Ramshaw B J, Vignolle B, Liang R, Hardy W N, Proust C and Bonn D A 2010 Angle-dependence of quantum oscillations in $YBa_2Cu_3O_{6.59}$ shows free spin behaviour of quasiparticles arXiv:1004.0260
[16] Chakravarty S, Laughlin R B, Morr D K and Nayak C 2001 Hidden order in the cuprates *Phys. Rev.* B **63** 094503
[17] Dimov I, Goswami P, Jia X and Chakravarty S 2008 Competing order, Fermi surface reconstruction, and quantum oscillations in underdoped high temperature superconductors *Phys. Rev.* B **78** 134529
[18] Chakravarty S, Sudbø A, Anderson P W and Strong S 1993 Interlayer tunneling and gap anisotropy in high-temperature superconductors *Science* **261** 337–40
[19] Andersen O K, Liechtenstein A I, Jepsen O and Paulsen F 1995 LDA energy bands, low-energy Hamiltonians, t', t'', $t_\perp(k)$, and $J_\perp$ *J. Phys. Chem. Solids* **56** 1573–91
[20] Sebastian S E, Harrison N, Goddard P A, Altarawneh M M, Mielke C H, Liang R, Bonn D A, Hardy W N, Andersen O K and Lonzarich G G 2010 Compensated electron and hole pockets in an underdoped high T_c superconductor arXiv:1001.5015
[21] Zheng G-Q, Clark W G, Kitaoka Y, Asayama K, Kodama Y, Kuhns P and Moulton W G 1999 Responses of the pseudogap and d-wave superconductivity to high magnetic fields in the underdoped high-T_c superconductor $YBa_2Cu_4O_8$: an NMR study *Phys. Rev.* B **60** R9947
[22] Klemm R A and Liu S H 1991 Intralayer-versus-interlayer pairing in the copper oxide superconductors *Phys. Rev.* B **44** 7526–45
[23] Pavarini E, Dasgupta I, Saha-Dasgupta T, Jepsen O and Andersen O K 2001 Band-structure trend in hole-doped cuprates and correlation with T_c max *Phys. Rev. Lett.* **87** 047003
[24] Feng D L *et al* 2001 Bilayer splitting in the electronic structure of heavily overdoped $Bi_2Sr_2CaCu_2O_{8+\delta}$ *Phys. Rev. Lett.* **86** 5550
[25] Nayak C 2000 Density-wave states of nonzero angular momentum *Phys. Rev.* B **62** 4880–9
[26] Shoenberg D 1984 *Magnetic Oscillations in Metals* (Cambridge: Cambridge University Press)
[27] Chakravarty S and Kee H-Y 2008 Fermi pockets and quantum oscillations of the Hall coefficient in high-temperature superconductors *Proc. Natl Acad. Sci. USA* **105** 8835–9
[28] Morinari T 2009 Pseudogap and short-range antiferromagnetic correlation controlled Fermi surface in underdoped cuprates: from Fermi arc to electron pocket *J. Phys. Soc. Japan* **78** 054708
[29] Jia X, Goswami P and Chakravarty S 2009 Resolution of two apparent paradoxes concerning quantum oscillations in underdoped high-T_c superconductors *Phys. Rev.* B **80** 134503–8
[30] Harrison N, McDonald R D and Singleton J 2007 Cuprate Fermi orbits and Fermi arcs: the effect of short-range antiferromagnetic order *Phys. Rev. Lett.* **99** 206406
[31] Harrison N 2009 Spin-density wave Fermi surface reconstruction in underdoped $YBa_2Cu_3O_{6+x}$ *Phys. Rev. Lett.* **102** 206405
[32] Yamaji K 1989 On the angle dependence of the magnetoresistance in quasi-two-dimensional organic superconductors *J. Phys. Soc. Japan* **58** 1520–3

[33] Kondo T *et al* 2009 Anomalous asymmetry in the Fermi surface of the high-temperature superconductor $YBa_2Cu_4O_8$ revealed by angle-resolved photoemission spectroscopy *Phys. Rev.* B **80** 100505
[34] Luttinger J M 1961 Theory of the de Haas–van Alphen effect for a system of interacting Fermions *Phys. Rev.* **121** 1251
[35] Abrikosov A A 1988 *Fundamentals of the Theory of Metals* (New York: Elsevier Science Publishers)
[36] Stephen M J 1992 Superconductors in strong magnetic fields: de Haas–van Alphen effect *Phys. Rev.* B **45** 5481
[37] Eun J, Jia X and Chakravarty S 2009 The surprising quantum oscillations in electron doped high temperature superconductors arXiv:0912.0728
[38] Garcia-Aldea D and Chakravarty S 2010 unpublished
[39] Luttinger J M 1960 Fermi surface and some simple equilibrium properties of a system of interacting Fermions *Phys. Rev.* **119** 1153
[40] Chubukov A V and Morr D K 1997 Electronic structure of underdoped cuprates *Phys. Rep.* **288** 355–87
[41] Dzyaloshinskii I 2003 Some consequences of the Luttinger theorem: the Luttinger surfaces in non-Fermi liquids and Mott insulators *Phys. Rev.* B **68** 085113
[42] Halperin B I, Lee Patrick A and Read N 1993 Theory of the half-filled Landau level *Phys. Rev.* B **47** 7312–43